Journal of Cleaner Production 346 (2022) 131144

Contents lists available at ScienceDirect

Journal of Cleaner Production

journal homepage: www.elsevier.com/locate/jclepro

Highly efficient isomerization of glucose to fructose over a novel aluminum doped graphitic carbon nitride bifunctional catalyst

Bo Cai [a,b,c], Junfeng Feng [a,b], Dayi Guo [a,b], Shuai Wang [a,b], Tianyi Ma [c], Thomas L. Eberhardt [d], Hui Pan [a,b,*]

[a] Jiangsu Co-Innovation Center for Efficient Processing and Utilization of Forest Resources, Nanjing Forestry University, 159 Longpan Road, 210037, Nanjing, PR China
[b] Jiangsu Province Key Laboratory of Green Biomass-based Fuels and Chemicals, Nanjing, 210037, PR China
[c] Centre for Translational Atomaterials, Faculty of Science, Engineering & Technology, Swinburne University of Technology, Hawthorn, Victoria, 3122, Australia
[d] Forest Products Laboratory, USDA Forest Service, One Gifford Pinchot Drive, Madison, WI, 53726, USA

ARTICLE INFO

Handling Editor: M.T. Moreira

Keywords:
Aluminum doped graphitic carbon nitride
Glucose
Fructose
Isomerization
γ-Valerolactone
Synergistic effect

ABSTRACT

Glucose isomerization to fructose is a crucial step for the efficient production of fuel and valuable chemicals from renewable carbohydrates. Aluminum (Al) was introduced into the structure of a graphitic carbon nitride (g-C_3N_4) by a simple thermal polycondensation of urea and aluminum chloride, and thereby, provided a series of Al-doped g-C_3N_4 (xAl-UCN) catalysts for the isomerization reaction. A high fructose yield of 48.29%, comparable to the quantitative yields (ca. 50%) by enzymatic routes, was achieved with the 0.5Al–UCN catalyst. Detailed characterizations of a series of Al–UCN catalysts, with different Al loadings, showed that 1) the Al loading amount has a profound effect on the physical-chemical properties of Al–UCN catalysts; 2) excess Al loading can inhibit the formation of a crystalline g-C_3N_4 structure; and 3) at lower Al loadings, the Al appears to be doped into the g-C_3N_4 framework possibly via coordination bonds. The mechanism for glucose isomerization to fructose may involve both Lewis acid and base catalyzed routes, with the coordinated Al species (Al[6]) providing Lewis acidity, and N-containing groups on g-C_3N_4 providing basicity. The additive effect of this dual-functionality is likely responsible for the high catalytic activity. The 0.5Al–UCN catalyst was readily recycled, demonstrating near-constant activity after 5 cycles of use. Altogether, glucose isomerization to fructose over the readily synthesized and recyclable Al–UCN catalyst could provide a highly-efficient and cost-effective step in lignocellulosic biomass valorization.

1. Introduction

Lignocellulosic biomass, as a renewable source of energy, has enormous potential to relieve the stress on declining non-renewable fossil energy supplies (Nie et al., 2020; Hou et al., 2018). Glucose is an essential carbohydrate that is abundantly available in nature in the form of cellulose, the primary biopolymer in lignocellulosic biomass (Mika et al., 2018). The isomerization of glucose to fructose is considered a key intermediate step in the production of biofuels and platform chemicals from lignocellulosic biomass given the fact that fructose can be converted to levulinic acid (LA), 5-hydroxymethylfurfural (HMF), and 2, 5-furandicarboxylic acid (FDCA), which are all important precursors for the production of plastics, green solvents, lubricants, and biofuels (Yabushita et al., 2019; Hou et al., 2021). The enzymatic conversion of glucose, commercialized for the production of high-fructose corn syrup, can provide a 42% yield of fructose (Buchholz and Seibel, 2008). However, this biocatalytic conversion generally suffers from high processing costs due to the short half-life of enzyme and reaction conditions that are sensitive to both temperature and pH. As for the isomerization of glucose via a chemical route, early investigations involved homogeneous inorganic bases (e.g., sodium hydroxide, calcium hydroxide) that are hampered by tedious substrates purification and/or catalyst recovery processes (Zhang et al., 2019; Carraher et al., 2015). Development of efficient heterogeneous catalysts for glucose isomerization are therefore of high interest.

Both heterogeneous Lewis acids and Brønsted bases have been applied for the isomerization of glucose to fructose. Among most reported Lewis acid catalysts for this reaction is Sn-Beta, a tin-containing molecular sieve with the zeolite beta topology, which possesses high

* Corresponding author. Jiangsu Co-Innovation Center for Efficient Processing and Utilization of Forest Resources, Nanjing Forestry University, 159 Longpan Road, 210037, Nanjing, PR China.
E-mail address: hpan@njfu.edu.cn (H. Pan).

https://doi.org/10.1016/j.jclepro.2022.131144
Received 5 October 2021; Received in revised form 20 February 2022; Accepted 24 February 2022
Available online 7 March 2022

Abbreviation list

UCN	Graphitic carbon nitride
Al–UCN	aluminum-doped graphitic carbon nitride
Fru	Fructose
Glu	Glucose
GVL	γ-Valerolactone
LA	Levulinic acid
MeOH	Methanol
THF	Tetrahydrofuran
Cp	The concentration of the product
np	The numbers of carbons in the product
nGlu	The numbers of carbons in the glucose
MW_p	The molecular mass of product
MW_{Glu}	The molecular mass of glucose
C_{Glui}	The initial and final concentrations of glucose
C_{Gluf}	The final concentrations of glucose

catalytic activity for glucose isomerization (Botti et al., 2020). A large-pore Sn-Beta achieved 31% fructose yield at 383 K in aqueous media (Moliner et al., 2010). Guo and co-workers reported that the stability of their Sn-Beta catalyst could be improved in dioxane/water reaction media and provide a 41.5% fructose yield (Guo et al., 2019). Compared with tin, aluminum (Al) is more abundant and lower in cost. Several Al species are well-known for their Lewis acidity such as Al(III) used in heterogeneous catalyst systems (Takagaki et al., 2014). Tsang and coworkers prepared a series of heterogeneous Al-based Lewis acid catalysts on different carbonaceous supports and the catalytic activities of these Al catalysts toward glucose isomerization achieved fructose yields as high as 34.6% (Yu et al., 2019a and b).

Heterogeneous basic catalysts have also been explored for the glucose isomerization to fructose. A solid base MgO was anchored on a high-area NbP support to obtain MgO/NbP catalysts which achieved 24.6% yield and 65.7% selectivity of fructose when isomerizing glucose at 393 K (Gao et al., 2019). A hydrotalcite (HT) catalyst with a Mg:Al ratio of 3:1 was reported to reach a fructose yield of up to 56% with 80% fructose selectivity (Yabushita et al., 2019). Finally, Otomo et al., used ammonia to treat various metal oxides to incorporate nitrogen into the structure of metal oxides (Otomo et al., 2019). They found that the catalytic activity and fructose selectivity of SiO_2 emerged after treatment with NH_3, indicating that nitrogen could be beneficial for the isomerization of glucose to fructose.

Graphitic carbon nitride (g-C_3N_4), a nitrogen-rich metal-free organic material that can be easily prepared from raw materials of low cost, possesses high thermal stability and high electron-transfer ability, but no toxicity (Zhang et al., 2020; Almeida Ribeiro et al., 2020). Graphitic carbon nitride is rich in N-containing species, such as amino groups (in the form of $–NH_2$ and –NH– groups) at the edge of graphitic sheets, and tertiary amines linking the heptazine rings (Fig. 1), all which could impart base properties to the surface of a g-C_3N_4 framework. A study on the photocatalytic cleavage of C–C bonds in lignin using mesoporous g-C_3N_4 as the catalyst suggested that the surface base sites (i.e., nitrogen species) on the g-C_3N_4 played similar role as that of photogenerated holes, removing hydrogen from the substrate and generating radical species, therefore promoting the activity of the catalyst (Liu et al., 2018). In addition, it has been reported that a g-C_3N_4 provided a promising catalyst support due to the fact that the 2D nanosheet structure of g-C_3N_4 promotes the dispersion and stabilization of metal particles, with the electron rich nitrogen modifying the electron density of the anchored metals, thereby contributing to the performance of the catalyst (Xu et al., 2018).

In this study, a series of Al-doped g-C_3N_4 catalysts were synthesized and evaluated for the isomerization of glucose to fructose. A green and recyclable solvent γ-valerolactone (GVL) was used as the preferred reaction medium and the isomerization was conducted at a moderate temperature 433 K, which are both beneficial for the environmental suitability of a biorefinery process. Prepared Al-doped g-C_3N_4 catalysts were then characterized in detail for their morphology, microstructure, and other physicochemical properties by XRD, TEM, XPS and solid-state NMR (^{13}C and ^{27}Al). The active species and reaction mechanisms were developed by scrutinizing the physicochemical properties and the corresponding performance of the isomerization reactions under different reaction conditions (e.g., temperature, time, and medium). The highest novelty and greatest impact of this work are that we prepared a bifunctional acid-base catalyst by introducing Al species with Lewis acidity into the structure of g-C_3N_4 that provides basicity. To the best of our knowledge, this is the first study involving the doping of Al species into the structure of g-C_3N_4 material and using the resulting Al-doped g-C_3N_4 as a bifunctional catalyst for the isomerization of glucose to fructose. The results from this study could provide an alternative strategy for designing catalytic materials needed for biomass conversions.

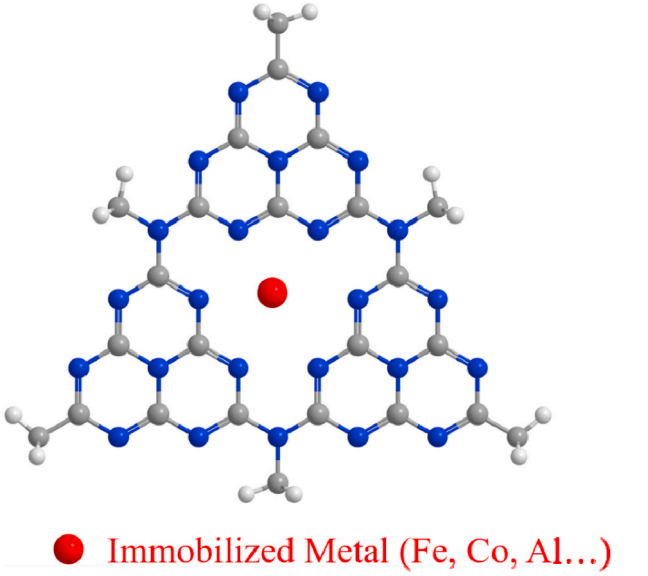

Fig. 1. General structure of catalysts based on metals coordinated with a graphitic carbon nitride (g-C_3N_4) framework.

2. Experimental section

2.1. Materials

Urea, $AlCl_3$, tetrahydrofuran (THF), methanol (MeOH), and cyclohexane were purchased from Sinopharm Chemical Reagent Company (Shanghai, China) and γ-valerolactone (GVL) was purchased from Energy Chemical Reagent Company (Shanghai, China). All chemicals were directly used without further purification.

2.2. Preparation of Al-doped g-C_3N_4 catalysts

The method to prepare the Al-doped g-C_3N_4 catalysts was adapted from a general method reported for preparing g-C_3N_4 nanosheets (Wu et al., 2020). As an example of a typical procedure, 0.5 g $AlCl_3{\cdot}6H_2O$ and 10 g of urea were dissolved in 100 mL deionized H_2O by stirring at 600 rpm for 6 h. The resulting solution was frozen at 253 K (overnight) before freeze drying to obtain the catalyst precursor. To generate the Al-doped g-C_3N_4 catalyst, the precursor was calcined at 823 K for 4 h in a muffle furnace (Anhui Kemi Machinery Technology Co., Ltd); a heating rate of 5 K min^{-1} was used to reach the calcining temperature. The resulting catalyst was collected as a yellow powder, and identified as

0.5Al–UCN. Four additional Al:urea (wt/wt) ratios of 0.25:10, 1:10, 1.5:10, and 2:10 were used to obtain Al-doped g-C_3N_4 catalysts identified as 0.25Al–UCN, 1.0Al–UCN, 1.5Al–UCN, and 2.0Al–UCN, respectively. A sample of g-C_3N_4 alone, identified as UCN, was obtained by direct calcination of urea under the same conditions as before.

2.3. Catalyst characterization

The crystalline structures of the catalysts were analyzed on an X-ray diffractometer (XRD, D/MAX III VC, Rigaku, Japan) using a Cu Kα ray source (λ = 0.1541 nm). The 2θ was recorded from 10° to 80° at a step speed of 5°/min, and the accelerating voltage and current were 40 kV and 40 mA, respectively.

The Brunauer−Emmett−Teller (BET) surface area, pore size, and pore volume of the catalysts were measured by an Automatic Surface Area and Pore Analyzer (Tristar II 3020 M, Micromeritics). The catalyst samples were degassed at 393 K for 12 h before analysis.

The real Al content of all samples were measured using an inductively coupled plasma-optical emission spectrometer (ICP-OES, Agilent 720 ES, USA) after digesting the samples in HNO_3/$HClO_4$, and diluting dissolved samples with deionized water. The Al contents were determined to be 3.75%, 7.51%, 9.40%, and 10.59%, for the 0.5Al–UCN, 1.0Al–UCN, 1.5Al–UCN, and the 2.0Al–UCN samples, respectively.

Fourier transform infrared (FT-IR) analyses of the catalysts were performed using a BRUKER VERTEX 80 V spectrometer (BRUKER, Germany). The spectra were recorded at room temperature using a spectral range of 4000 to 400 cm^{-1} and a resolution of 2 cm^{-1}.

The microstructure of the catalysts were analyzed by transmission electron microscopy (TEM, JEOL-2100, Japan) at an accelerating voltage of 200 kV. The catalyst samples were dispersed in ethanol and then one drop of dispersed sample was deposited on a carbon-coated grid. The elemental composition of the catalyst was evaluated by TEM coupled with energy dispersive X-ray spectroscopy (EDX). Scanning electron microscopy (SEM) analysis was conducted on a JSM-7600F electron microscope (JEOL, Japan) to assess the morphology of the catalysts.

The surface chemical states of the catalysts were analyzed by X-ray photoelectron spectrometry (XPS) on an AXIS UltraDLD X-ray photoelectron spectrometer (SHIMADZU, Japan) with Al Kα X-ray as the excitation source (hν = 1486.6 eV). The Al and C atoms chemical environment were analyzed by solid-state magic angle spinning (MAS) NMR at room temperature on a AVANCE III WB 400 MHz spectrometer.

CO_2- and NH_3-temperature-programmed-desorption (TPD) measurements were performed with a Micromeritics Auto Chem II 2920 device. For each run, the sample was first heated to 573 K at a rate of 10 K min^{-1} under He flow for 0.5 h to remove adsorbed impurities. Then it was cooled to 323 K to adsorb CO_2 or NH_3 followed by a He (1 h) to remove physically adsorbed CO_2 or NH_3. TPD data from 323 K to 823 K was collected with a slope of 20 K min^{-1}.

2.4. Catalytic conversion of glucose over Al-doped g-C_3N_4 catalysts

For a typical glucose isomerization reaction used in this study, glucose (0.1 g), catalyst (0.05 g), and solvent (12 mL) were added to a 35 mL stainless steel reactor (Anhui Kemi Machinery Technology Co., Ltd) with a magnetic stirrer. The reactor was sealed, purged with N_2 three times to remove the air inside, and then heated to 433 K, maintaining this temperature for 4 h under an atmosphere of 0.5 MPa N_2. The reactor was then cooled to room temperature, and the reaction mixture was sampled for analysis. All isomerization reactions were carried out in triplicate for each catalyst. For the investigation of catalyst recycling, the catalyst was collected by centrifugation after each run followed by 3 washings with GVL to clean the catalyst. The washed catalyst was transferred to the reactor with the fresh GVL which was used directly as the reaction solvent to minimize the loss of catalyst.

2.5. Analysis of reaction products

The reaction products were analyzed by high-performance liquid chromatography (HPLC) (Agilent 1260, USA) equipped with an Aminex Bio-Rad HPX-87H column (Bio-Rad Laboratories, USA). Sulfuric acid (5 mM) was used as the mobile phase at a flow rate of 0.6 mL/min and the column temperature was kept at 323 K. The product yield (Equation (1)), product selectively (Equation (2)), and glucose conversion (Equation (3)) values were calculated as follows:

$$\text{Product yield (mol\%)} = \frac{C_p \times \frac{n_p}{MW_p}}{C_{Glui} \times \frac{n_{Glu}}{MW_{Glu}}} \times 100 \quad (1)$$

$$\text{Product selectively (mol\%)} = \frac{C_p \times \frac{n_p}{MW_p}}{(C_{Glui} - C_{Gluf}) \times \frac{n_{Glu}}{MW_{Glu}}} \times 100 \quad (2)$$

$$\text{Glucose conversion (mol\%)} = \frac{(C_{Glui} - C_{Gluf})}{C_{Glui}} \times 100 \quad (3)$$

where C_p is the concentration of the product (mg/ml); n_p and n_{Glu} are numbers of carbons in the corresponding product and glucose, respectively; MW_p and MW_{Glu} are the molecular mass of the corresponding product and glucose, respectively; and C_{Glui} and C_{Gluf} are the initial and final concentrations of glucose (mg/ml), respectively.

3. Results and discussion

3.1. Characterization of Al-doped g-C_3N_4 catalysts

The crystalline structures of the UCN and the Al–UCN samples were characterized by X-ray diffraction spectroscopy (XRD); the spectra are shown in Fig. 2a. The two diffraction peaks at 2θ of 13.0° and 27.14° correspond to the (100) and (002) planes of the g-C_3N_4 framework, which represent the in-plane structural packing of tri-s-triazine (heptazine) units and the interlayer stacking of g-C_3N_4 sheets, respectively (Ma et al., 2021). The intensities of these two peaks decreased with increased Al loading. This suggested that the loading of Al had a negative impact on g-C_3N_4 crystallinity. In addition, the diffraction peak of the (002) plane (i.e., 2θ at 27.14°) became a wide peak when the Al:urea ratio was higher than 1.5:10, indicating that excessive Al doping would prevent the formation of a crystalline g-C_3N_4 structure. The inset plot in Fig. 2a shows the enlarged area of 2θ around 27° in the spectra of the UCN and 0.5Al–UCN samples. Compared to UCN, the diffraction peak of the (002) plane in the 0.5Al–UCN sample shifted to 27.54°. A similar shift was observed for the 1.0Al–UCN sample. Some studies have reported that metal doping could cause a greater lattice distortions and interplanar distance between graphic sheets of g-C_3N_4 and therefore result in the shifting of their diffraction peaks (Wang et al., 2009; Dong et al., 2021).

No peaks corresponding to aluminum metal, aluminum oxide, aluminum nitrides, or aluminum carbides are present in the spectra of 0.5Al–UCN and 1.0Al–UCN. Similar results were reported by several studies on different metals, including Fe-, Cu-, and Co-doped g-C_3N_4 materials. It was suggested that this phenomenon was attributed to the chemical coordination of the metal species with the g-C_3N_4 host in the form of metal-N bonds (Wang et al., 2009; Zhang et al., 2015). The two very small peaks between 10° and 20° in the spectra of 1.5Al–UCN and 2.0Al–UCN could be related to some of the above-mentioned Al species. For the Al–UCN catalysts with higher Al loading, in addition to doping into the structure of g-C_3N_4, the excessive amount of Al could form other Al species on the surface of g-C_3N_4, thereby increasing the complexity of the XRD pattern, especially for 1.5Al–UCN and 2.0Al–UCN. Considering the similar XRD results in this study, it could be inferred that appropriate amount metal aluminum might also coordinate with the nitrogen rich g-C_3N_4 matrix and form Al–N bonds in the Al–UCN samples prepared in this study.

The UCN and Al–UCN samples with different Al loadings were

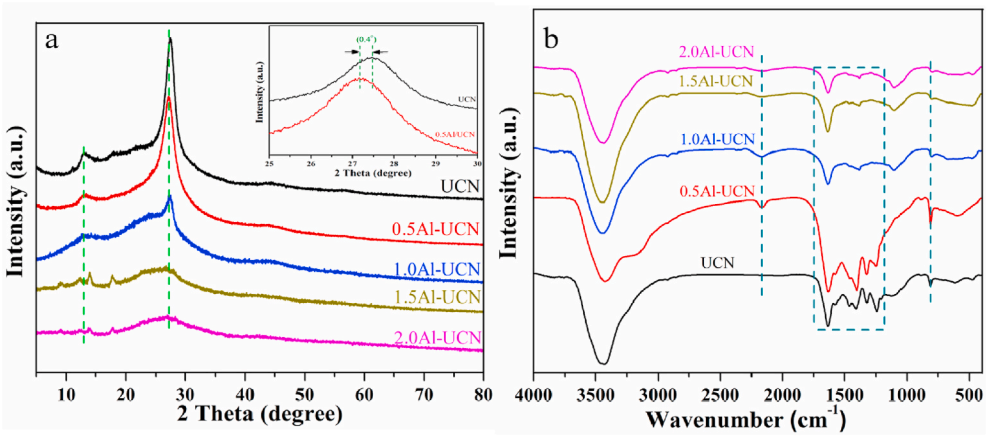

Fig. 2. (a) XRD and (b) FT-IR spectra of UCN and also the Al–UCN samples prepared with different Al loadings.

analyzed by FT-IR spectroscopy (Fig. 2b) and showed the UCN and 0.5Al–UCN samples to have similar spectra. The peak at 810 cm^{-1} can be assigned to the out-of-plane bending of heptazine rings and the peaks at 1200 to 1800 cm^{-1} can be assigned to the stretching modes of aromatic C–N heterocycles (Liang et al., 2015). Except for 0.5Al–UCN, peaks from ranges of 1200–1800 cm^{-1} in the spectra of the other Al–UCN samples became much weaker, attributed to the less-ordered heptazine ring structure of these samples caused by excessive levels of aluminum used for doping. This result is in agreement with that from the XRD analysis. A small new peak at 2170 cm^{-1} appeared in the spectra of most Al–UCN samples and is tentatively assigned to N≡C- groups (Yu et al., 2017; Zou et al., 2020). This result suggests that the doping of Al could introduce defects in the ordered placement of the nitrogen in the g-C_3N_4 framework (Zhao et al., 2019). Finally, the peaks at 3000-3500 cm^{-1} region of all the UCN and Al–UCN spectra can readily be assigned to N–H stretching vibrations (Liang et al., 2015).

The morphology and element distribution of the UCN and Al–UCN samples were analyzed by SEM and TEM. The SEM images (Fig. 3 and Fig. S1) show that the UCN, 0.5Al–UCN and 1.0Al–UCN samples all have a planar structures although the two Al–UCN samples seem to have less ordered appearance. On the other hand, the 1.5Al–UCN and 2.0Al–UCN samples display a totally different dense blocky structure (Figs. S1c and S1d). Further observation shows that the 0.5Al–UCN sample has thinner sheet structure than the UCN sample (Fig. 3b). In addition, some curly thin pieces are observed in the 0.5Al–UCN sample, which should be resulted from the low surface energy of the thin sheet structure.

The TEM images for the UCN and 0.5Al–UCN samples suggest a stacked thin layer structure (Fig. 3c and d) while the other Al–UCN samples with higher amounts of Al doping show a dense stacked structure (Figs. S2a–S2c). Thus, only a moderate amount of Al doping retains the basic morphology of g-C_3N_4. The high resolution TEM images also confirm the similarity between the morphologies of the UCN and 0.5Al–UCN samples (Fig. S3). Finally, the TEM-EDS mapping analysis showed that Al is highly dispersed in the g-C_3N_4 structure of the 0.5Al–UCN sample (Fig. 3e and f).

The N_2 adsorption-desorption isotherm shows that both the UCN and Al–UCN samples display a type IV isotherm (Fig. S4), which suggests they are mesoporous materials according to IUPAC classification. The textural and structural properties of the UCN and Al–UCN samples are listed in Table S1. It can be seen that the specific surface areas of Al–UCN samples decreased as the amount of Al doping increased (Jiang et al., 2021). This result is consistent with the dense structures shown in the SEM images for the Al–UCN samples with high Al loadings. Given the Al content of 3.75% measured by ICP-OES, the 0.5Al–UCN sample still has a specific surface area and pore size (Fig. S4d) similar to those of the UCN sample, thereby indicating that Al is doped within the g-C_3N_4 framework as opposed to being dispersed on the surface or in the pores between nanosheets.

The chemical states of the elements presented on the UCN and Al–UCN samples were further investigated by XPS analysis. The C 1s XPS spectra are shown in Fig. 4a and Fig. S5. As for 0.5Al–UCN, two peaks at binding energies of 284.8 eV and 288.4 eV are attributed to the sp^2 hybridized graphitic carbon (C–C) and sp^2 bonded carbon in the aromatic heterocycle (N–C═N) of the g-C_3N_4, respectively, which is also considered to be the major carbon in the skeleton of the conjugated system (Zhang et al., 2012). Compared to the UCN sample, the binding energies of N–C═N in the Al–UCN samples all slightly shifted to the high field region. A small peak at 286.1 eV belongs to C-NH_x or –C≡N (Ren et al., 2020). Meanwhile, the N 1s spectra of UCN could be deconvoluted into three major peaks located at 398.4 eV, 399.5 eV, and 400.9 eV, which correspond to C═N–C, N-$(C)_3$, and C-NH_x bonding structures, respectively (Fig. 4b). In addition, the binding energies of C═N–C and N-$(C)_3$ for 0.5Al–UCN shifted to higher energy fields than those of UCN, which is similar to the shift of the binding energies of C═N–C in the C 1s spectra (Fig. 4a). Similar phenomena have been reported by Gao and co-workers in their study on Fe-doped g-C_3N_4 nanosheets used as a photocatalyst (Gao et al., 2017). They suggested that the shifting of binding energies of N and C atoms on a Fe-doped g-C_3N_4 nanosheets was attributed to the formation of Fe–N coordinate bonds. Therefore, it could be speculated that Al–N coordinate bonds might be also formed in the Al–UCN catalysts of this study, which caused the binding energies of C═N–C and N-$(C)_3$ in the C 1s and N 1s spectra, respectively, to shift to higher fields for the Al–UCN catalysts (Gao et al., 2017; Yu et al., 2017). Specifically, the doped Al atoms provide unoccupied molecular orbitals for bonding, while N atoms in the heptazine rings provide lone pair electrons. Therefore, the electron density of N atoms decreased, as did the C atoms, due to the conjugated structure of the heptazine ring (Gao et al., 2017). The decrease in electron density resulted in the higher binding energy of corresponding N and C species. Other than these three major peaks, a weak peak at a binding energy of 404.1 eV, indexed to π-excitation or the charging effect in the cyano-group and heterocycles, appears in the spectra of the UCN and 0.5Al–UCN samples, but was absent in the spectra of Al–UCN samples with higher amounts of Al doping; this further supports the likelihood of excess Al preventing the formation of the g-C_3N_4 framework (Zhu et al., 2018; Zhang et al., 2012). On the other hand, the O 1s spectrum (Fig. S5) remained the same as that of the UCN support, indicating O had no interactions with other elements after Al doping.

The Al 2p spectra of the Al–UCN sample are shown in Fig. 4c and Fig. S5c. Four major peaks could be deconvoluted at the binding energies of 73.8 eV, 74.5 eV, 75.2 eV, and 76.1 eV, assigned to γ-AlO(OH) (Kloprogge et al., 2006), γ-$Al(OH)_3$/Al–O–C (Yu et al., 2019b), β-$Al(OH)_3$ (Kloprogge et al., 2006), and Al_2O_3 (Bicker et al., 1985), respectively. It should be noted that a peak located at binding energy of

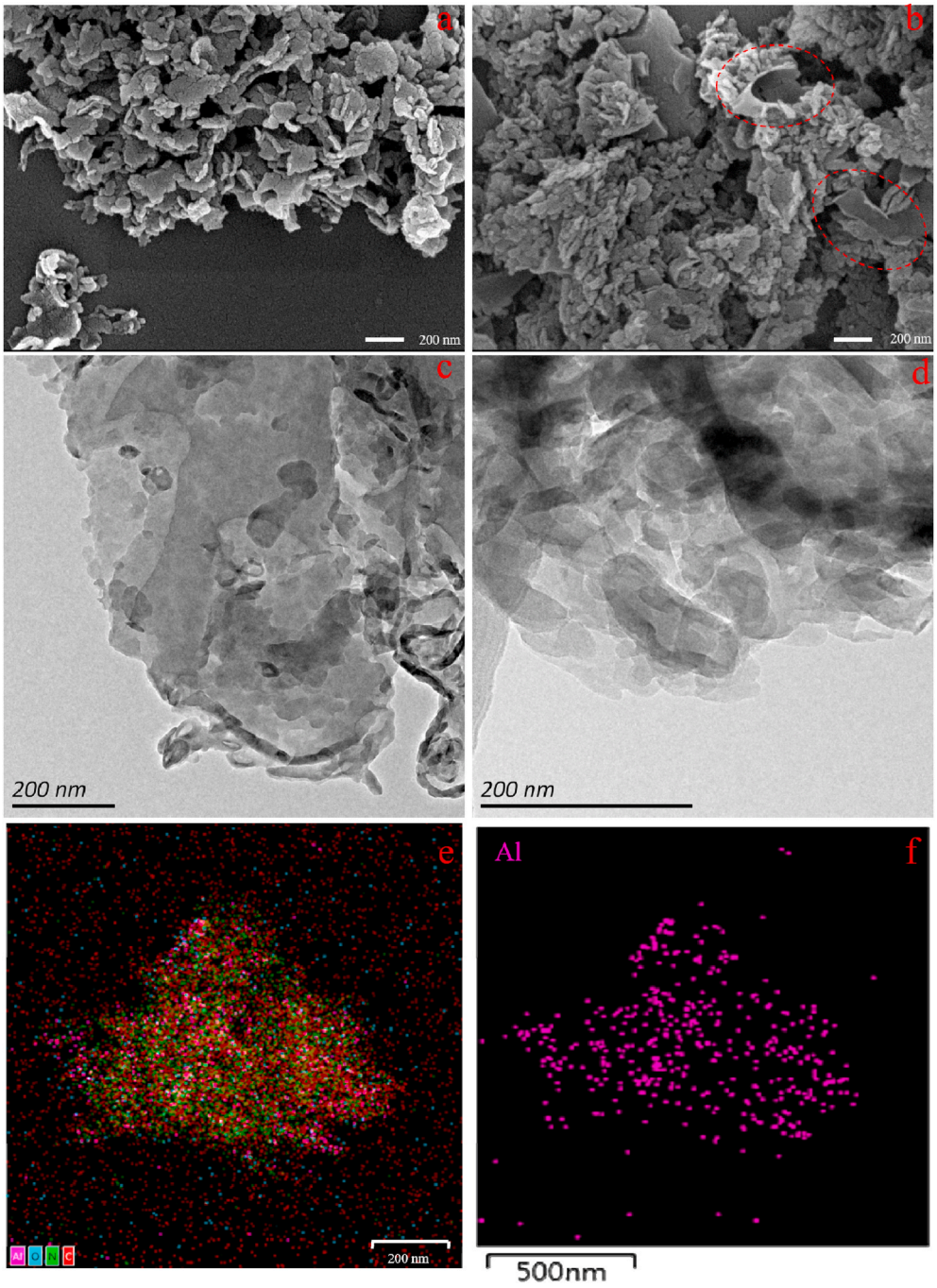

Fig. 3. SEM images of (a) UCN, (b) 0.5Al–UCN and TEM images of (c) UCN, (d) 0.5Al–UCN; TEM-Mapping image of (e) 0.5Al–UCN and (f) Al distribution of 0.5Al–UCN (UCN: graphitic carbon nitride from urea, Al–UCN: Al-doped graphitic carbon nitride).

77.3 eV, corresponding to four- or six-coordinated Al species (Al[4] or Al [6]), is present in the spectrum of the 0.5Al–UCN catalyst. A tiny signal at the same binding energy is observed in the spectrum of 1.0Al–UCN while it is absent in the spectra of 1.5Al–UCN and 2.0Al–UCN. It is known that the structure of g-C_3N_4 contains a cavity filled with lone-pair electrons from six neighboring nitrogen. It is considered an ideal site for metal inclusion (Wang et al., 2009). As suggested by the XRD and FT-IR results above, only 0.5Al–UCN retained the basic g-C_3N_4 structure which could provide cavities for Al to form Al–N coordination. Therefore, 0.5Al–UCN is the only Al–UCN catalyst having coordinated Al species alone.

The 0.5Al–UCN sample was subjected to ^{27}Al MAS NMR analysis to further confirm the chemical environments of the doped Al. In the ^{27}Al NMR (Fig. 4d), curve fitting gave signals at 80.5 and 27.1 ppm, corresponding to four- (Al[4]) and five- (Al[5]) coordinated Al, respectively (Yu et al., 2019b; Vinod Chandran et al., 2019); peaks at −7.6, −44.9 and −117.3 ppm are assigned to six- (Al[6], Al[6]* and Al[6]$^{\#}$, respectively) coordinated Al (Yu et al., 2019a; Xiong et al., 2020). Notably, the six-coordinated Al species (Al[6], Al[6]* and Al[6]$^{\#}$) are the dominant species in the 0.5Al–UCN catalyst, indicating that Al species were complexed with g-C_3N_4 through N_6-donor ligands in its electron rich cavities (Wang et al., 2018). Meanwhile, the ^{13}C NMR spectra of UCN and 0.5Al–UCN are shown in Fig. S5d in which two peaks, located at 155.9 and 163.2 ppm, are present in both spectra. The first peak belongs to the C atoms in the melem structure and the latter peak corresponds to sp^2 hybridized C in the form of N–C═N, which is the

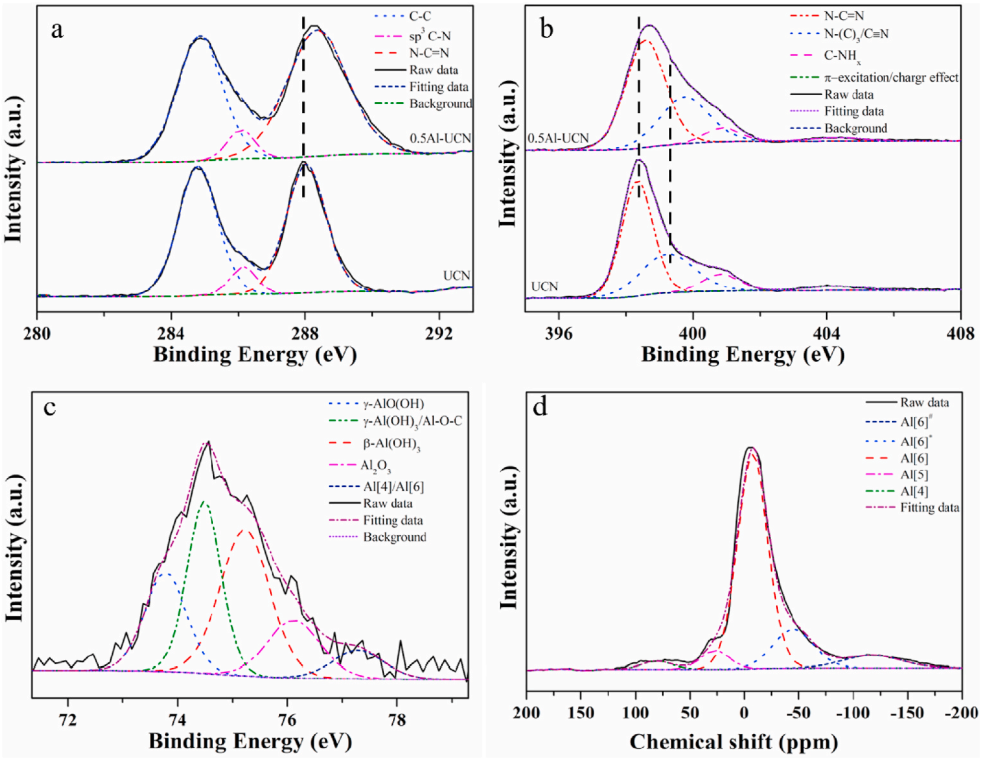

Fig. 4. XPS spectra (a) C 1s, (b) N 1s of UCN and 0.5Al–UCN, and (c) Al 2p; (d) ^{27}Al NMR spectra of 0.5Al–UCN (UCN: graphitic carbon nitride from urea, Al–UCN: Al-doped graphitic carbon nitride).

major carbon type present in an aromatic carbon nitride (Zhang et al., 2015). Since no signals corresponding to Al–C bond are observed in the spectra of 0.5Al–UCN, it appears that the aluminum interactions are primarily with nitrogen in the carbon nitride (Zhang et al., 2015). It should also be noted that the chemical shift of the carbon in 0.5Al–UCN is almost identical to that of UCN. Namely, no obvious changes occurred after Al doping, which suggests that Al atoms are anchored in the cavity of g-C_3N_4 though interacting with nitrogen without breaking its tri-s-triazine ring structure.

3.2. Isomerization of glucose to fructose over Al–UCN catalysts

3.2.1. Initial catalyst screening

The catalytic activities of the Al–UCN catalysts for the isomerization of glucose to fructose was evaluated and the results summarized in Table 1. The UCN control (urea calcined alone) had a 11.59% fructose yield and 30.55% glucose conversion using GVL as the solvent (entry 1). It is known that g-C_3N_4 materials possess N-rich groups, such as –NH_2 on their external structures, which would impart base catalysis functionality sufficient for the isomerization of glucose to fructose (Liu et al., 2014). Compared to the UCN control, the fructose yield increased sharply from 11.59% to 37.38% over the 0.25Al–UCN catalyst, which showed that the aluminum species played an important role in the isomerization reaction. As the amount of doped aluminum increased, the yield of fructose first increased (entry 3) and then decreased (entry 4). Lower fructose yields were obtained with the Al–UCN catalysts with the highest Al doping (entries 5 and 6). Note that Al_2O_3 could be as a Lewis acid catalyst (Hou et al., 2019); when applied in this isomerization reaction, the yield of fructose was only 7.6% (entry 11).

Catalyst 0.5Al–UCN exhibited the highest catalytic activity for glucose isomerization reaction among all the Al–UCN catalysts prepared in this study. Based on the characterization results from previous sections, there could be two reasons for the high catalytic activity of the 0.5Al–UCN catalyst. First, the 0.5Al–UCN catalyst had the highest specific surface area along with an excellent pore structure (Table S1 and Fig. S5); these features likely promoted the contact between the substrate and the active sites (Yu et al., 2019b). Second, the six-coordinated Al species in the 0.5Al–UCN catalyst provided Lewis acidity for the glucose isomerization into fructose beyond any base catalysis imparted by the g-C_3N_4 structure itself (Yu et al., 2019a).

Reaction medium also plays a crucial role for the product yield and selectivity. Several common solvents, including both protic and aprotic, were investigated for the isomerization of glucose with the 0.5Al–UCN catalyst. The results show that protic solvents such as H_2O and MeOH (entries 9 and 10, respectively) gave lower fructose yields and

Table 1
Isomerization of glucose to fructose with different catalysts and solvent. [a].

Entry	Catalyst	Solvent	Fru. Yield (%)	LA Yield (%)	Glu. Conv. (%)	Fru. Sel. (%)
1	UCN	GVL	11.59	15.37	30.55	37.94
2	0.25Al–UCN	GVL	37.38	6.5	81.84	45.67
3[b]	0.5Al–UCN	GVL	48.29	14.97	67.[b]	.65
4	1.0Al–UCN	GVL	34.24	19	71.49	47.89
5	1.5Al–UCN	GVL	5.26	5.1	49.8	10.56
6	2.0Al–UCN	GVL	3.55	5.1	64.66	5.5
7	0.5Al–UCN	THF	41.54	–	88.38	47.00
8	0.5Al–UCN	H_2O	12.73	–	77.35	16.46
9	0.5Al–UCN	MeOH	27.52	–	100	27.52
10	Al_2O_3	GVL	7.6	9.0	94.49	8.04
11	UCN + Al_2O_3	GVL	18.7	14.6	90.3	20.7
12[c]	0.5Al/UCN	GVL	–	5.4	–	–

[a] Reaction condition: 0.1 g glucose, 0.05 g 0.5Al–UCN, 12 mL solvent, 433 K, 4 h, 0.5 MPa N_2.
[b] 3 h.
[c] Without glucose. (UCN: graphitic carbon nitride from urea, Al–UCN: Al-doped graphitic carbon nitride, Fru.: fructose, Glu.: glucose, LA: levulinic acid, GVL: γ-Valerolactone, THF: tetrahydrofuran, MeOH: methanol).

selectivities than aprotic solvents such as GVL and THF (entries 3 and 8, respectively) under identical reaction conditions, which might be due to the fact that GVL and THF can dissolve by-products (e.g. humins) produced in the reaction that might otherwise block the active sites on the catalyst (Yan et al., 2017). Aside from the highest fructose yield and selectivity being achieved with GVL as the reaction solvent, the use of GVL is advantageous since it is an environmentally friendly and renewable green solvent that can be obtained from biomass.

3.2.2. Effects of reaction conditions

The isomerization of glucose to fructose over 0.5Al–UCN was further optimized using GVL as the reaction solvent by manipulating the reaction temperature, time, catalyst dosage, and reaction pressure (Fig. 5). It shown in Fig. 5a, the conversion of glucose increased gradually from 43.2% to 86.4% as the reaction temperature increased from 393 K to 453 K. The yields of fructose were instead all similar except that at 433 K for which the yield was twice that at the other temperatures. As for the fructose selectivity, that varied for the three lowest temperatures and dropped sharply for the 453 K reaction temperature. The decreases in the fructose yield and selectivity with the highest temperature can be attributed to the formation of by-products (e.g., humins) as observed in other transformations of glucose (Garces et al., 2018).

The effects of reaction time on the isomerization reaction were also assessed using a constant reaction temperature of 433 K (Fig. 5b). By increasing the reaction time, the glucose conversions gradually increased. Slight, decreases in fructose yield and selectivity for reaction times longer than 3 h can be attributed to the possible cross- and/or self-polymerizations between reaction products and reactant and/or intermediates (Danon et al., 2014; Zhang et al., 2020). With respect to the reaction time, the highest fructose yield (48.29%) and selectivity (71.65%) values were obtained at 3 h.

Whereas the previous manipulations of the reaction temperature and time used a 50 mg dosage of the 0.5Al–UCN catalyst, we then investigated the effect of different catalyst dosages ranging from 20 mg to 60 mg (Fig. 5c). The reaction with 20 mg catalyst dosage provided 41.0% fructose yield and 66.2% glucose conversion. As the catalyst dosages were increased, the fructose yields barely increased in a stepwise manner; the highest fructose yield and selectivity were obtained with 50 mg catalyst dosage. When the catalyst dosage further increased to 60 mg, the fructose yield and selectivity slightly decreased, possibly owing to the excessive active sites that accelerated the side reactions (e.g., condensation and rehydration) (Yang et al., 2017).

Finally, the reaction pressure demonstrated little effect on the yield of fructose (Fig. 5d), which was expected given the high boiling point of the reaction solvent, GVL (Horváth et al., 2008; Alonso et al., 2013). Using the optimized reaction conditions for the isomerization of glucose to fructose over the 0.5Al–UCN catalyst, those being a reaction temperature of 433 K, reaction time of 3 h, catalyst dosage of 50 mg, and N_2 pressure of 0.5 MPa, the fructose yield was 48.29% and the fructose selectivity was 71.65% with 67.4% glucose being converted in the process. This high fructose yield (48.29%) is comparable to that from enzymatic isomerization of glucose (Buchholz and Seibel, 2008; Bhosale et al., 1996).

It should be noted that the yield of the main by-product of this reaction, levulinic acid (LA), was kept at about 14% under most reaction conditions. Wang et al. reported that GVL could undergo ring opening reaction to produce LA in the presence of Lewis acid sites (Wang et al., 2017). A blank reaction with the 0.5Al–UCN catalyst in GVL without glucose yielded 5.4% LA (Table 1, entry 12), thereby demonstrating that the majority of the LA obtained in reactions with glucose was indeed derived from conversions of said glucose. Since LA is also considered a high value-added biomass-derived platform compound, the conversion of glucose over the 0.5Al–UCN catalyst to valuable products could provide a total yield of 63.26% fructose and LA under optimized reaction conditions.

3.2.3. Comparison with representative studies

Table 2 provides a list showing the catalytic performance of several Al/carbon-based catalysts for glucose isomerization that are reported in the literature. Two results with the 0.5Al–UCN catalyst are provided for

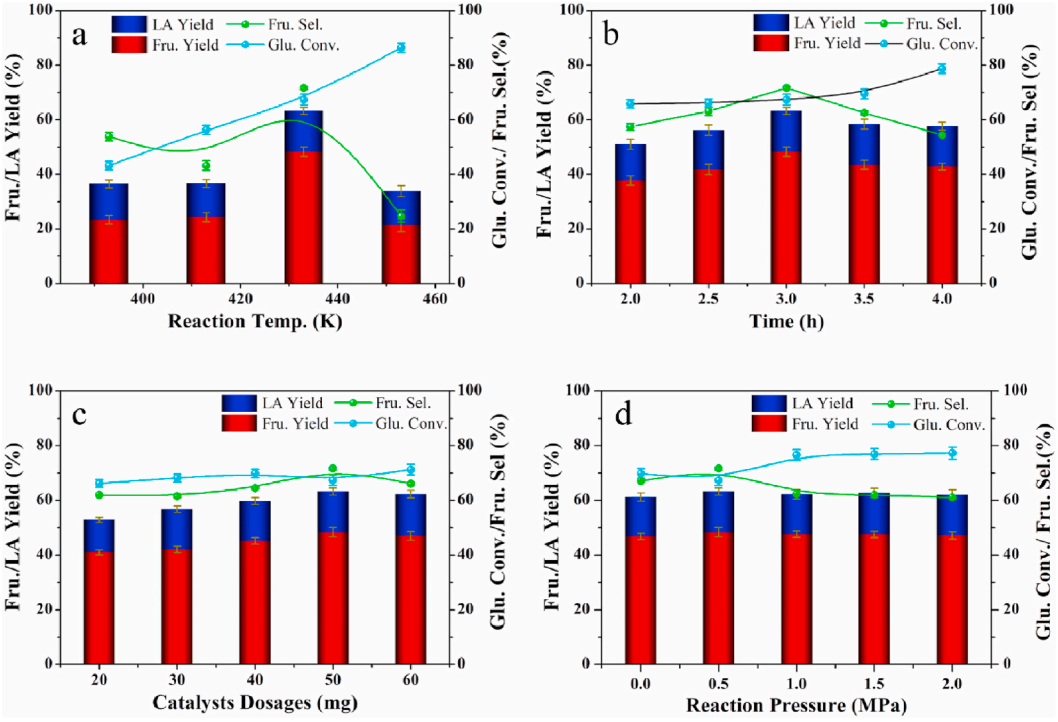

Fig. 5. Glucose conversion, fructose yield and selectivity resulting from the catalytic conversion of glucose over 0.5Al–UCN (a) at different reaction temperatures, (b) at different reaction times at 433 K, (c) with different catalysts dosages at 433 K, and (d) at different reaction pressures (reaction conditions: 0.1 g glucose and 0.05 g 0.5Al–UCN in 12 mL GVL). (Al–UCN: Al doped graphitic carbon nitride, Fru.: fructose, Glu.: glucose, LA: levulinic acid, GVL: γ-Valerolactone).

Table 2
Comparison of representative studies on glucose isomerization to fructose over Al-based catalyst.

Catalyst	Fructose yield (%)	Al content (%)	Fructose Selectivity (%)	[f]$m_{glu.}/m_{cat.}$	Solvent	Ref.
[a]Al-Biochar	21.5	13.1	73.8	2	Water	Yu et al. (2019b)
[b]GIO-Al	34.6	5.9	63.4	2	Acetone/H_2O	Yu et al. (2019a)
[c]$Al_{10\%}$/HC220–K_2CO_3	32.58	11.71	93.3	2	Water	Zhang et al. (2020)
[d]Al-Hydrochar	13.4	13.48	77.8	2	Water	Sheng et al. (2019)
[e]Al/HC-300	25	16.2	59.4	2.5	Acetone/H_2O	Liu et al. (2021)
0.5Al–UCN	48.29	3.75	71.65	2	GVL	This work
0.5Al–UCN	35.6	3.75	67.94	4	GVL	This work

[a] Biochar supported Al.
[b] Graphene oxide supported Al.
[c] Hydrochar supported Al treated by K_2CO_3.
[d] Cellulose derived hydrochar supported Al.
[e] Hydrochar supported Al treated at 573 K.
[f] Ratio of mass of glucose (m_{glu}) and mass of catalyst (m_{cat}). (Fru.: fructose, Glu.: glucose, LA: levulinic acid, GVL: γ-Valerolactone).

comparison. Our catalyst (0.5Al–UCN) gave highest fructose yield for the glucose isomerization reaction among all the listed Al/carbon-based catalysts; having the lowest Al content (3.75%) of all these catalysts, 0.5Al–UCN also exhibited a superior aluminum atomic economy. In addition, a reaction doubling the glucose loading (glucose/catalyst = 200 mg/50 mg) was conducted, and achieved a 35.6% fructose yield, demonstrating the efficiency of the 0.5Al–UCN catalyst. At both glucose loading levels, the 0.5Al–UCN catalyst achieved a fructose selectivity that was comparable to literature-reported catalysts. Briefly, it should also be noted that 0.5Al–UCN catalyst provided comparable results to other types of catalysts (such as Sn-β, HT et al.) as listed in Table S3.

3.2.4. Stability of catalyst

The recyclability of the 0.5Al–UCN catalyst was evaluated using the optimized reaction conditions (0.1 g glucose and 0.05 g 0.5Al–UCN in 12 mL GVL, 3 h at 433 K). After each run, the catalyst was separated by centrifuge, washed with fresh GVL and then directly subjected to next run. Upon repetitive uses, it can be seen that the glucose conversion, fructose yield and fructose selectivity remained essentially constant over 5 runs (Fig. 6) and so the 0.5Al–UCN catalyst has excellent stability for glucose isomerization.

To further explore the persistent catalytical activity, the 0.5Al–UCN catalyst after three runs (identified as R0.5Al–UCN) was collected and characterized by XRD, FT-IR spectroscopy, and XPS (Fig. 7). The XRD spectrum of R0.5Al–UCN exhibited a similar diffraction pattern with that of fresh 0.5Al–UCN catalyst (Fig. 7a), suggested that the crystalline structure of the 0.5Al–UCN catalyst remained intact after the isomerization reaction. Similar to the XRD result of fresh 0.5Al–UCN catalyst, no diffraction peaks from any Al species appeared in the spectrum of R0.5Al–UCN, thereby indicating that the doped Al species are quite stable during the catalytic reaction. The results from FT-IR and TEM characterizations (Fig. 7b and Fig. S2d, respectively) further confirm the stable structure of the R0.5Al–UCN catalyst.

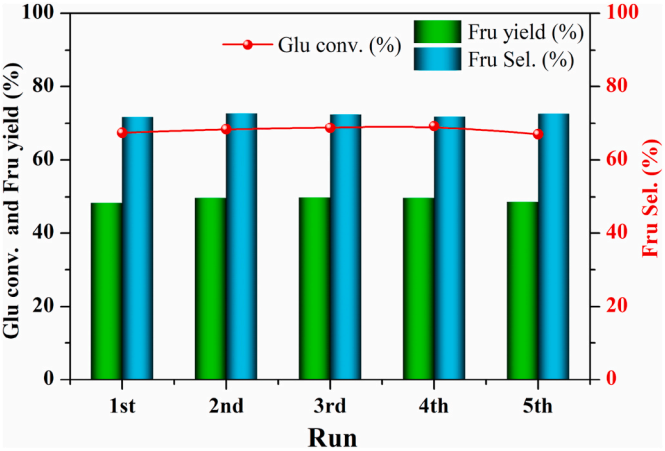

Fig. 6. Catalytic performance of recovered 0.5Al–UCN. (Reaction conditions: 0.1 g glucose and 0.05 g 0.5Al–UCN in 12 mL GVL, 433 K, 3 h). (Al–UCN: Al-doped graphitic carbon nitride, Fru.: fructose, Glu.: glucose, GVL: γ-Valerolactone).

The XPS C 1s and N 1s spectra (Fig. S6) of the R0.5Al–UCN catalyst suggests it to have the same carbon and nitrogen species as those on 0.5Al–UCN. For the XPS Al 2p spectrum (Fig. 7c), the peaks located at 77.3 eV corresponded to the isomerization active sites (tetrahedral or octahedral coordinated Al (Al[4] or Al[6])) (Yu et al., 2019a) indicating almost no change in the Al species after three isomerization reactions. Thus, the results of the catalyst recycling experiments, and characterization results of R0.5Al–UCN, confirm that the Al[4] or Al[6] sites play a crucial role in the glucose isomerization reaction.

3.3. Possible mechanism of glucose isomerization over Al–UCN catalysts

Based on the characterizations of the Al–UCN catalysts, and their catalytic performance, possible reaction mechanisms for glucose isomerization to fructose are provided in Scheme 1. Given the co-existence of Lewis acid and base active sites on the Al doped g-C_3N_4 catalysts (i.e., 0.5Al–UCN), the glucose isomerization may occur via two reaction routes. The first route (route I in Scheme 1) involves the hydrogen transfer from C-2 to C-1 mediated by the basic sites on the catalyst, whereby the α-hydroxy C-2 is deprotonated by the base to form a 1,2-enediol intermediate followed by the electron pair at C-2 moving via the carbon skeleton to C-1 to form the corresponding α-hydroxy ketone (Nagorski and Richard, 2001; Moliner et al., 2010). The second route (route II in Scheme 1) follows an intramolecular hydride shift between C-2 and C-1 mediated by the Al species with adequate Lewis acidity, especially the coordinated Al[4] or Al[6]) species on the 0.5Al–UCN catalyst (Qi et al., 2019; Yu et al., 2019a). It is worth noting that the 0.5Al–UCN catalyst, with both acid and base sites, exhibited higher catalytic activity than the base alone catalyst (i.e., UCN, Table 1, entry 1) or acid alone catalyst (i.e., Al_2O_3, Table 1, entry 11), indicating a possible additive effect with both Lewis acid and base sites being available. Physical mixing of the UCN and Al_2O_3 catalysts and subjecting them to the reaction provided a lower fructose yield (18.7%) than the 0.5Al–UCN catalyst, suggesting that the Al-doped g-C_3N_4 framework formed during the calcification process is critical to isomerization reaction. Further study will be necessary to determine if there are synergistic aspects between the Lewis acid and base functionalities present in catalyst system.

4. Conclusions

In this study, Al-doped g-C_3N_4 materials were prepared by thermal polycondensation of urea and aluminum chloride ($AlCl_3$) and applied as

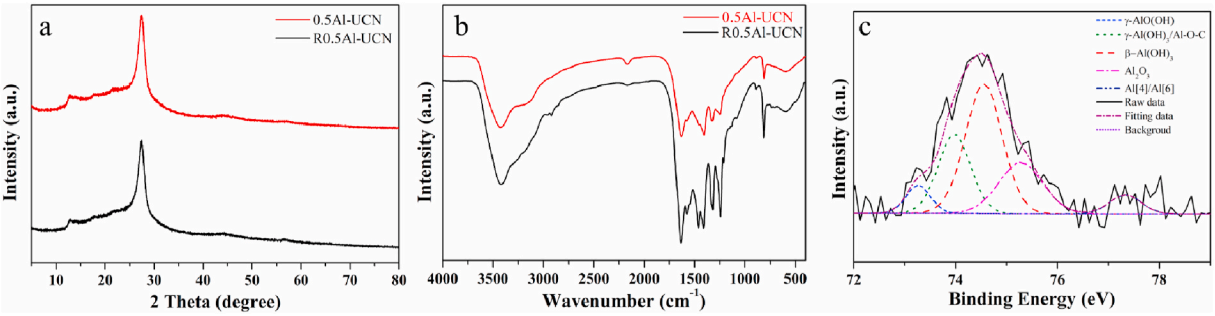

Fig. 7. (a) XRD, (b) FT-IR and (c) XPS Al 2p spectra of 0.5Al–UCN and R0.5Al–UCN. (Al–UCN: Al-doped graphitic carbon nitride, R0.5Al–UCN: recovered 0.5Al–UCN catalyst).

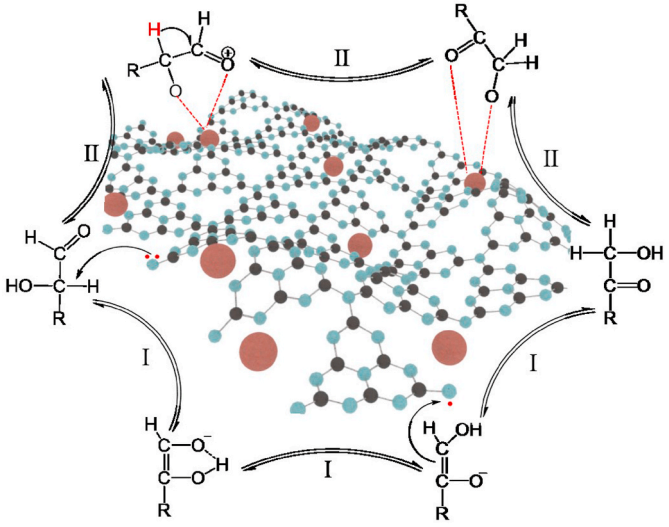

Scheme 1. Proposed reaction mechanisms for isomerization of glucose over the 0.5Al–UCN catalyst.

a novel catalyst for the efficient isomerization of glucose to fructose in a green and recyclable solvent GVL. The Al loading amount in the preparation process showed a profound effect on the physicochemical properties of the Al–UCN catalysts. The 0.5Al–UCN displayed similar crystalline structure and morphological features as those of a g-C_3N_4 prepared by the thermal polycondensation of urea; excess Al loading inhibited the formation of the g-C_3N_4 structure. Based on the characterizations of the 0.5Al–UCN catalyst, it is speculated that Al could present in the g-C_3N_4 framework via Al–N coordination bonds; for 0.5Al–UCN catalyst, six-coordinated Al (Al[6]) was the dominant Al species present. Isomerization reactions showed that g-C_3N_4 (UCN) itself had some catalytic activity. The highest fructose yield (48.29%) and selectivity (71.65%), under at optimal reaction conditions, was achieved with the 0.5Al–UCN catalyst having an Al content of 3.75 wt%. Based on our results, it is proposed the isomerization of glucose occurs via both base and Lewis acid catalyzed reaction routes via the nitrogen-containing groups of the g-C_3N_4 framework and the coordinated Al species within, respectively. Given that the 0.5Al–UCN catalyst exhibited essentially the same catalytic activity after 5 reaction cycles, this stable Al-doped g-C_3N_4 catalyst shows promise for glucose isomerization and has potential for other applications in the conversion of biomass to high value-added products.

CRediT authorship contribution statement

Bo Cai: Conceptualization, Methodology, Writing – original draft, preparation. **Junfeng Feng:** Visualization, Supervision. **Dayi Guo:** Investigation, Software. **Shuai Wang:** Validation, Data curation. **Tianyi Ma:** Visualization, Supervision. **Thomas L. Eberhardt:** Writing – review & editing. **Hui Pan:** Project administration, Funding acquisition, Writing – review & editing.

Declaration of competing interest

The authors declare that they have no known competing financial interests or personal relationships that could have appeared to influence the work reported in this paper.

Acknowledgements

The authors are grateful for the financial support from National Natural Science Foundation of China (No.31770631) and National Natural Science Foundation of China (No.32101469). CB thanks the financial support of A Project Funded by the National First-class Disciplines (PNFD).

Appendix A. Supplementary data

Supplementary data to this article can be found online at https://doi.org/10.1016/j.jclepro.2022.131144.

References

Almeida Ribeiro, R.S., Monteiro Ferreira, L.E., Rossa, V., Lima, C.G.S., Paixão, M.W., Varma, R.S., Melo Lima, T., 2020. Graphitic carbon nitride-based materials as catalysts for the upgrading of lignocellulosic biomass-derived molecules. ChemSusChem 13, 3992–4004. https://doi.org/10.1002/cssc.202001017.

Alonso, D.M., Wettstein, S.G., Dumesic, J.A., 2013. Gamma-valerolactone, a sustainable platform molecule derived from lignocellulosic biomass. Green Chem. 15, 58–595. https://doi.org/10.1039/c3gc37065h.

Bhosale, S.H., Rao, M.B., Deshpande, V.V., 1996. Molecular and industrial aspects of glucose isomerase. Microbiol. Rev. 60, 280–300. https://doi.org/10.1128/mmbr.60.2.280-300.1996.

Bicker, R., Deger, H., Herzog, W., Rieser, K., Pulm, H., Hohlneicher, G., Freund, H.-J., 1985. X-ray photoelectron spectroscopy study of silica-alumina catalysts used for a new pyridine synthesis. J. Catal. 94, 69–78. https://doi.org/10.1016/0021-9517(85)90083-1.

Botti, L., Kondrat, S.A., Navar, R., Padovan, D., Martinez-Espin, J.S., Meier, S., Hammond, C., 2020. Solvent-activated hafnium-containing zeolites enable selective and continuous glucose-fructose isomerisation. Angew. Chem. 132, 20192–20198. https://doi.org/10.1002/ange.202006718.

Buchholz, K., Seibel, J., 2008. Industrial carbohydrate biotransformations. Carbohydr. Res. 343, 1966–1979. https://doi.org/10.1016/j.carres.2008.02.007.

Carraher, J.M., Fleitman, C.N., Tessonnier, J.P., 2015. Kinetic and mechanistic study of glucose isomerization using homogeneous organic brønsted base catalysts in water. ACS Catal. 5, 3162–3173. https://doi.org/10.1021/acscatal.5b00316.

Danon, B., Marcotullio, G., de Jong, W., 2014. Mechanistic and kinetic aspects of pentose dehydration towards furfural in aqueous media employing homogeneous catalysis. Green Chem. 16, 39–54. https://doi.org/10.1039/C3GC41351A.

Dong, H., Zuo, Y., Song, N., Hong, S., Xiao, M., Zhu, D., Sun, J., Chen, G., Li, C., 2021. Bimetallic synergetic regulating effect on electronic structure in cobalt/vanadium co-doped carbon nitride for boosting photocatalytic performance. Appl. Catal. B Environ. 287, 119954. https://doi.org/10.1016/j.apcatb.2021.119954.

Gao, D.M., Shen, Y.B., Zhao, B., Liu, Q., Nakanishi, K., Chen, J., Kanamori, K., Wu, H., He, Z., Zeng, M., Liu, H., 2019. Macroporous niobium phosphate-supported

magnesia catalysts for isomerization of glucose-to-fructose. ACS Sustain. Chem. Eng. 7, 8512–8521. https://doi.org/10.1021/acssuschemeng.9b00292.
Gao, J., Wang, Y., Zhou, S., Lin, W., Kong, Y., 2017. A facile one-step synthesis of Fe-doped g-C_3N_4 nanosheets and their improved visible-light photocatalytic performance. ChemCatChem 9, 1708–1715. https://doi.org/10.1002/cctc.201700492.
Garces, D., Faba, L., Diaz, E., Ordonez, S., 2018. Aqueous phase transformation of glucose into HMF and levulinic acid combining homogeneous and heterogeneous catalysis. ChemSusChem 12, 924–934. https://doi.org/10.1002/cssc.201802315.
Guo, Q., Ren, L., Alhassan, S.M., Tsapatsis, M., 2019. Glucose isomerization in dioxane/water with Sn-β catalyst: improved catalyst stability and use for HMF production. Chem. Commun. 55, 14942–14945. https://doi.org/10.1039/c9cc07842h.
Horváth, I.T., Mehdi, H., Fábos, V., Boda, L., Mika, L.T., 2008. γ-Valerolactone-a sustainable liquid for energy and carbon-based chemicals. Green Chem. 10, 238–324. https://doi.org/10.1039/b712863k.
Hou, Q., Qi, X., Zhen, M., Qian, H., Nie, Y., Bai, C., Zhang, S., Bai, X., Ju, M., 2021. Biorefinery roadmap based on catalytic production and upgrading 5-hydroxymethylfurfural. Green Chem. 23, 119–231. https://doi.org/10.1039/d0gc02770g.
Hou, Q., Zhen, M., Li, W., Liu, L., Liu, J., Zhang, S., Nie, Y., Bai, C., Bai, X., Ju, M., 2019. Efficient catalytic conversion of glucose into 5-hydroxymethylfurfural by aluminum oxide in ionic liquid. Appl. Catal. B Environ. 253, 1–10. https://doi.org/10.1016/j.apcatb.2019.04.003.
Hou, Q., Zhen, M., Liu, L., Chen, Y., Huang, F., Zhang, S., Li, W., Ju, M., 2018. Tin phosphate as a heterogeneous catalyst for efficient dehydration of glucose into 5-hydroxymethylfurfural in ionic liquid. Appl. Catal. B Environ. 224, 183–193. https://doi.org/10.1016/j.apcatb.2017.09.049.
Jiang, F.Y., Zhou, Y.H., Chen, R., Liu, T.T., Luo, J.Y., Huang, Y.B., 2021. In-situ fabrication of Ag nanoparticles on biomass derived biochar as highly active catalyst for the halogenation of terminal alkynes at room temperature. Appl. Surf. Sci. 560, 150039. https://doi.org/10.1016/j.apsusc.2021.150039.
Kloprogge, J.T., Duong, L.V., Wood, B.J., Frost, R.L., 2006. XPS study of the major minerals in bauxite: gibbsite, bayerite and (pseudo-)boehmite. J. Colloid Interface Sci. 296, 572–576. https://doi.org/10.1016/j.jcis.2005.09.054.
Liang, Q., Li, Z., Huang, Z.H., Kang, F., Yang, Q.H., 2015. Holey graphitic carbon nitride nanosheets with carbon vacancies for highly improved photocatalytic hydrogen production. Adv. Funct. Mater. 25, 6885–6892. https://doi.org/10.1002/adfm.201503221.
Liu, C., Carraher, J.M., Swedberg, J.L., Herndon, C.R., Fleitman, C.N., Tessonnier, J.P., 2014. Selective base-catalyzed isomerization of glucose to fructose. ACS Catal. 4, 4295–4298. https://doi.org/10.1021/cs501197w.
Liu, H., Li, H., Lu, J., Zeng, S., Wang, M., Luo, N., Xu, S., Wang, F., 2018. Photocatalytic cleavage of C-C bond in lignin models under visible light on mesoporous graphitic carbon nitride through π-π stacking interaction. ACS Catal. 8, 4761–4771. https://doi.org/10.1021/acscatal.8b00022.
Liu, J., Zhang, Xiaoliang, Yang, L., Danhassan, U.A., Zhang, S., Yang, M., Sheng, K., Zhang, Ximing, 2021. Glucose isomerization catalyzed by swollen cellulose derived aluminum-hydrochar. Sci. Total Environ. 777, 146037. https://doi.org/10.1016/j.scitotenv.2021.146037.
Ma, J., Jin, D., Li, Y., Xiao, D., Jiao, G., Liu, Q., Guo, Y., Xiao, L., Chen, X., Li, X., Zhou, J., Sun, R., 2021. Photocatalytic conversion of biomass-based monosaccharides to lactic acid by ultrathin porous oxygen doped carbon nitride. Appl. Catal. B Environ. 283, 119520. https://doi.org/10.1016/j.apcatb.2020.119520.
Mika, L.T., Cséfalvay, E., Németh, Á., 2018. Catalytic conversion of carbohydrates to initial platform chemicals: chemistry and sustainability. Chem. Rev. 118, 505–613. https://doi.org/10.1021/acs.chemrev.7b00395.
Moliner, M., Román-Leshkov, Y., Davis, M.E., 2010. Tin-containing zeolites are highly active catalysts for the isomerization of glucose in water. Proc. Natl. Acad. Sci. U.S.A. 107, 6164–6168. https://doi.org/10.1073/pnas.1002358107.
Nagorski, R.W., Richard, J.P., 2001. Mechanistic imperatives for aldose-Ketose isomerization in water: specific, general base- and metal ion-catalyzed isomerization of glyceraldehyde with proton and hydride transfer. J. Am. Chem. Soc. 123, 794–802. https://doi.org/10.1021/ja003433a.
Nie, Y., Hou, Q., Bai, C., Qian, H., Bai, X., Ju, M., 2020. Transformation of carbohydrates to 5-hydroxymethylfurfural with high efficiency by tandem catalysis. J. Clean. Prod. 274, 123023. https://doi.org/10.1016/j.jclepro.2020.123023.
Otomo, R., Fujimoto, M., Nagao, M., Kamiya, Y., 2019. Ammonia-treated metal oxides as base catalysts for selective isomerization of glucose in water. Mol. Catal. 475, 110479. https://doi.org/10.1016/j.mcat.2019.110479.
Qi, T., He, M.F., Zhu, L.F., Lyu, Y.J., Yang, H.Q., Hu, C.W., 2019. Cooperative catalytic performance of Lewis and brønsted acids from $AlCl_3$ salt in aqueous solution toward glucose-to-fructose isomerization. J. Phys. Chem. C 123, 4879–4891. https://doi.org/10.1021/acs.jpcc.8b11773.
Ren, W., Cheng, J., Ou, H., Huang, C., Anpo, M., Wang, X., 2020. Optimizing the crystallization process of conjugated polymer photocatalysts to promote electron transfer and molecular oxygen activation. J. Catal. 389, 636–645. https://doi.org/10.1016/j.jcat.2020.07.005.
Sheng, K., Zhang, S., Liu, J., E, S., Jin, C., Xu, Z., Zhang, X., 2019. Hydrothermal carbonization of cellulose and xylan into hydrochars and application on glucose isomerization. J. Clean. Prod. 237, 117831. https://doi.org/10.1016/j.jclepro.2019.117831.
Takagaki, A., Jung, J.C., Hayashi, S., 2014. Solid Lewis acidity of boehmite γ-AlO(OH) and its catalytic activity for transformation of sugars in water. RSC Adv. 4, 43785–43791. https://doi.org/10.1039/c4ra08061k.
Vinod Chandran, C., Kirschhock, C.E.A., Radhakrishnan, S., Taulelle, F., Martens, J.A., Breynaert, E., 2019. Alumina: discriminative analysis using 3D correlation of solid-state NMR parameters. Chem. Soc. Rev. 48, 134–156. https://doi.org/10.1039/c8cs00321a.
Wang, X., Chen, X., Thomas, A., Fu, X., Antonietti, M., 2009. Metal-containing carbon nitride compounds: a new functional organic-metal hybrid material. Adv. Mater. 21, 1609–1612. https://doi.org/10.1002/adma.200802627.
Wang, Y., Mao, J., Meng, X., Yu, L., Deng, D., Bao, X., 2018. Catalysis with two-dimensional materials confining single atoms: concept, design, and applications. Chem. Rev. 119, 1806–1854. https://doi.org/10.1021/acs.chemrev.8b00501.
Wang, Y., Zhang, P., Huang, G., Yuan, Q., Guan, Y., Wu, P., 2017. Facile synthesis of ethyl-4-ethoxy pentanoate as a novel biofuel additive derived from γ-valerolactone. ACS Sustain. Chem. Eng. 5, 6645–6653. https://doi.org/10.1021/acssuschemeng.7b00891.
Wu, J., Zhang, Y., Zhou, J., Wang, K., Zheng, Y.Z., Tao, X., 2020. Uniformly assembling n-type metal oxide nanostructures (TiO_2 nanoparticles and SnO_2 nanowires) onto P doped g-C_3N_4 nanosheets for efficient photocatalytic water splitting. Appl. Catal. B Environ. 278, 119301. https://doi.org/10.1016/j.apcatb.2020.119301.
Xiong, X., Yu, I.K.M., Tsang, D.C.W., Chen, L., Su, Z., Hu, C., Luo, G., Zhang, S., Ok, Y.S., Clark, J.H., 2020. Study of glucose isomerisation to fructose over three heterogeneous carbon-based aluminium-impregnated catalysts. J. Clean. Prod. 268, 122378. https://doi.org/10.1016/j.jclepro.2020.122378.
Xu, X., Luo, J., Li, L., Zhang, D., Wang, Y., Li, G., 2018. Unprecedented catalytic performance in amine syntheses: via Pd/g-C_3N_4 catalyst-assisted transfer hydrogenation. Green Chem. 20, 2038–2046. https://doi.org/10.1039/c8gc00144h.
Yabushita, M., Shibayama, N., Nakajima, K., Fukuoka, A., 2019. Selective glucose-to-fructose isomerization in ethanol catalyzed by hydrotalcites. ACS Catal. 9, 2101–2109. https://doi.org/10.1021/acscatal.8b05145.
Yan, L., Yao, Q., Fu, Y., 2017. Conversion of levulinic acid and alkyl levulinates into biofuels and high-value chemicals. Green Chem. 19, 5527–5547. https://doi.org/10.1039/c7gc02503c.
Yang, T., Zhou, Y.H., Zhu, S.Z., Pan, H., Huang, Y.B., 2017. Insight into aluminum sulfate-catalyzed xylan conversion into furfural in a γ-valerolactone/water biphasic solvent under microwave conditions. ChemSusChem 10, 4066–4079. https://doi.org/10.1002/cssc.201701290.
Yu, H., Shi, R., Zhao, Yunxuan, Bian, T., Zhao, Yufei, Zhou, C., Waterhouse, G.I.N., Wu, L. Z., Tung, C.H., Zhang, T., 2017. Alkali-Assisted synthesis of nitrogen deficient graphitic carbon nitride with tunable band structures for efficient visible-light-driven hydrogen evolution. Adv. Mater. 29, 1–7. https://doi.org/10.1002/adma.201605148.
Yu, Iris K.M., Xiong, X., Tsang, D.C.W., Ng, Y.H., Clark, J.H., Fan, J., Zhang, S., Hu, C., Ok, Y.S., 2019a. Graphite oxide- and graphene oxide-supported catalysts for microwave-assisted glucose isomerisation in water. Green Chem. 21, 4341–4353. https://doi.org/10.1039/c9gc00734b.
Yu, Iris K.M., Xiong, X., Tsang, D.C.W., Wang, L., Hunt, A.J., Song, H., Shang, J., Ok, Y.S., Poon, C.S., 2019b. Aluminium-biochar composites as sustainable heterogeneous catalysts for glucose isomerisation in a biorefinery. Green Chem. 21, 1267–1281. https://doi.org/10.1039/c8gc02466a.
Zhang, G., Huang, C., Wang, X., 2015. Dispersing molecular cobalt in graphitic carbon nitride frameworks for photocatalytic water oxidation. Small 11, 1215–1221. https://doi.org/10.1002/smll.201402636.
Zhang, G., Zhang, J., Zhang, M., Wang, X., 2012. Polycondensation of thiourea into carbon nitride semiconductors as visible light photocatalysts. J. Mater. Chem. 22, 8083–8091. https://doi.org/10.1039/c2jm00097k.
Zhang, N., Meng, X.G., Wu, Y.Y., Song, H.J., Huang, H., Wang, F., Lv, J., 2019. Highly selective isomerization of glucose into fructose catalyzed by a mimic glucose isomerase. ChemCatChem 11, 2355–2361. https://doi.org/10.1002/cctc.201900143.
Zhang, Q., Xiang, X., Ge, Y., Yang, C., Zhang, B., Deng, K., 2020. Selectivity enhancement in the g-C_3N_4-catalyzed conversion of glucose to gluconic acid and glucaric acid by modification of cobalt thioporphyrazine. J. Catal. 388, 11–19. https://doi.org/10.1016/j.jcat.2020.04.027.
Zhang, S., Sheng, K., Liang, Y., Liu, J., E, S., Zhang, X., 2020. Green synthesis of aluminum-hydrochar for the selective isomerization of glucose to fructose. Sci. Total Environ. 727, 138743. https://doi.org/10.1016/j.scitotenv.2020.138743.
Zhang, Y., Feng, J., Xiao, Z., Liu, Y., Ma, H., Wang, Z., Pan, H., 2020. Highly efficient and selectivefractionation strategy for lignocellulosic biomass with recyclable dioxane/ethylene glycol binary solvent. Ind. Crop. Prod. 144, 112038. https://doi.org/10.1016/j.indcrop.2019.112038.
Zhao, D., Dong, C., Wang, B., Chen, C., Huang, Y., Diao, Z., Li, S., Guo, L., Shen, S., 2019. Synergy of dopants and defects in graphitic carbon nitride with exceptionally modulated band structures for efficient photocatalytic oxygen evolution. Adv. Mater. 31, 1903545. https://doi.org/10.1002/adma.201903545.
Zhu, Z., Pan, H., Murugananthan, M., Gong, J., Zhang, Y., 2018. Visible light-driven photocatalytically active g-C_3N_4 material for enhanced generation of H_2O_2. Appl. Catal. B Environ. 232, 19–25. https://doi.org/10.1016/j.apcatb.2018.03.035.
Zou, J., Yu, Y., Qiao, K., Wu, S., Yan, W., Cheng, S., Jiang, N., 2020. Microwave synthesis of phosphorus-doped graphitic carbon nitride nanosheets with enhanced electrochemiluminescence signals. J. Mater. Sci. 55, 13618–13633. https://doi.org/10.1007/s10853-020-04862-6.